Environmental Science Nano

Biological Impact of Nanoscale Lithium Intercalating Complex Metal Oxides to Model Bacterium *Bacillus subtilis*

Journal:	*Environmental Science: Nano*
Manuscript ID	EN-ART-09-2018-000995.R2
Article Type:	Paper
Date Submitted by the Author:	22-Nov-2018
Complete List of Authors:	Feng, Z. Vivian ; Augsburg College, Chemistry Department Miller, Blake ; Augsburg College Linn, Taylor; Augsburg College Pho, Thomas; Augsburg College Hoang, Khoi Nguyen; Augsburg College Hang, Mimi; University of Wisconsin Madison Mitchell, Stephanie; University of Minnesota, Chemistry Hernandez, Rodrigo; Augsburg College Carlson, Erin; University of Minnesota, Chemistry Hamers, Robert; University of Wisconsin-Madison, Department of Chemistry

Environmental Significance

Nanoscale complex metal oxides are a class of emerging nanomaterials widely used in energy storage and catalysis applications. Although these materials are produced in increasing quantities, there are few incentives or infrastructure for recycling currently, which poses questions for their environmental impact upon disposal at the end of their life cycles. This work examines the biological impact to a model environmentally beneficial bacterium by a class of lithium intercalating battery cathode materials in terms of bacterial growth, metabolic respiration, spore formation, antibiotic production, as well as DNA damage. This initial attempt at probing the genotoxicity of these nanomaterials guide us towards an understanding of their toxicity mechanism at a molecular level, and provides insights into material redesign.

Journal Name

ARTICLE

Biological Impact of Nanoscale Lithium Intercalating Complex Metal Oxides to Model Bacterium *Bacillus subtilis*

Received 00th January 20xx,
Accepted 00th January 20xx

DOI: 10.1039/x0xx00000x

www.rsc.org/

Z. Vivian Feng[a]*, Blake R. Miller[a], Taylor G. Linn[a], Thomas Pho[a], Khoi Nguyen L. Hoang[a] , Mimi N. Hang[b], Stephanie L. Mitchell[c], Rodrigo Tapia Hernandez[a], Erin E. Carlson[c], Robert J. Hamers[b]

As lithium intercalating complex metal oxides become more widely used in energy storage devices, there is an increasing need to understand their environmental impact at the end of their life cycle due to the lack of recycling options. In this study, we examine the biological impact of a panel of nanoscale lithium nickel manganese cobalt oxides ($Li_xNi_yMn_zCo_{1-y-z}O_2$, 0 < x, y, z < 1, abbreviated as NMCs), to a model Gram-positive bacterium, *Bacillus subtilis* in terms of cellular respiration and growth. A highly sensitive single-cell gel electrophoresis method is also applied for the first time to understand the genotoxicity of this nanomaterial to bacterial cells. Results from these assays indicate that the free Ni and Co ions released from the incongruent dissolution of the NMC material in *B. subtilis* growth media induced both hindered growth and cellular respiration. More remarkably, the DNA damage induced by the combination of the two ions in solution is comparble to that induced by the NMC material, which suggests the free Ni and Co ions are responsible for the toxicity observed. A material redesign by enriching Mn is also presented. The combined approaches of evaluating impact on bacterial growth, respiration, DNA damage at a single-cell level, as well as other phenotypical changes allows us to probe the nanomaterial and bacterial cells from a mechanistic prospective, and provides a useful means to an understanding of bacterial response to new potential environmental stressors.

Introduction

As the effort to reduce greenhouse gas emission continues, electric vehicles have expanded from a technological novelty to consumer products, largely enabled by the development of lithium ion battery technology.[1,2] Lithium intercalation compounds, often used in the cathodes of these batteries, are under active development in order to improve on energy density, charging current, power, safety, and to reduce cost. [3–5] Recently, these complex metal oxides have also demonstrated potentials in catalysis applications.[6]

Lithium nickel manganese cobalt oxides ($Li_xNi_yMn_zCo_{1-y-z}O_2$, 0 < x, y, z < 1) known as the NMCs, are a class of complex metal oxides that share the same layered material structure as the commercialized lithium cobalt oxide (LCO). They offer high energy density, improved stability and more cycle times. [7] The most common composition of $Li_xNi_{1/3}Mn_{1/3}Co_{1/3}O_2$ (NMC-111) (x = 1 indicating full lithiation) has been used in commercial electric vehicles, such as the Nissan Leaf and BMW i3.[1] The framework of the material features nanoscale layers that enable improved lithium diffusion, better wettability, and good process ability. [2,7] Mechanical stress from repeated charging and discharging cycles have also resulted in nanometer scale fractures.[8,9] In addition to the NMC-111 composition, by varying the ratios of the starting material, researchers have been able to develop other compositions of NMCs, as well as explore their functions in an effort to boost performance and reduce costs.[10] For instance, Ni-enriched NMCs, e.g. NMC-622, have shown promising performance enhancement as the cathode material and is going into full scale production.[1,7,11]

In spite of the active research in the development of high performing complex metal oxides, due to the lack of infrastructure and incentives for recycling, the majority of these materials will end up in the environment in landfills or aquatic systems at the end of their usage.[12–14] Therefore, in order to understand the potential interactions between these nanomaterials with environmental biological models, a few recent studies have focused on the impacts of these nanosheets with model lipid membranes[15], a model Gram-negative bacterium, *Shewanella oneidensis*[8,16], and a model multicellular aquatic organism, *Daphnia magna*.[17] These early studies have indicated that metal ions released from nanosheet dissolution as the primary means of toxicity to some biological species.

Building on the earlier findings, and in order to gain a molecular level insight into the toxicity mechanism, in this study, we examine the impacts of NMC on the metabolic respiration and DNA damage to a Gram-positive model bacterium, *Bacillus subtilis*. In addition to the fact that *B. subtilis* is one of the most

[a] Chemistry Department, Augsburg University, Minneapolis, MN 55454.
[b] Department of Chemistry, University of Wisconsin, Madison, WI 53706.
[c] Department of Chemistry, University of Minnesota, Minneapolis, MN 55455

Electronic Supplementary Information (ESI) available: [details of any supplementary information available should be included here]. See DOI: 10.1039/x0xx00000x

well-studied gram positive bacterial model, wild type strain SB491 used in this work is commonly found in soils, and is critical to many nutrient cycles in the environment. Low concentrations of metal ions are often required by bacteria as essential nutrients. However, high levels of metal ions may lead to non-specific binding interactions with proteins and cellular receptors, resulting in the disruption of biochemical pathways, DNA damage, and toxicity to bacteria.[18] In particular, while Ni and Co ions from the NMC nanosheets have brought environmental concerns[14], studies have shown that some bacterial species may play a role in metal remediation in the environment through biosorption.[19,20] Therefore, we are interested in examining the interactions of these complex metal oxides with a model bacterial species.

Bacteria are generally considered a trophic group to be highly impacted by metal-based nanomaterials based on prior studies.[8,16,21] This study aims to broaden the understanding of the impact of nanoscale layered lithium intercalating materials on the environment using an environmentally relevant model bacterium, *B. subtilis*, to provide molecular insights into the mechanism of toxicity. The biological impacts of the NMC material, as well as the dissolved ions will be assessed in terms of bacterial respiration, growth, and DNA breakage. Upon understanding the sources of toxicity, an effort to redesign the NMC material in order to reduce its toxicity is also reported.

Experimental

Synthesis and characterizations of Li-intercalating battery materials

NMC nanosheets were synthesized using previously reported methods and the same batch of Mn-enriched NMC nanosheets used in the present study was also previously used in other publications.[8] Briefly, the metal hydroxides are made via controlled precipitation. The hydroxides are then converted to the lithiated oxides by heating in a molten salt flux, leading to nanoflakes approximately 5-7 nm thick and with lateral dimensions of approximately 80-120 nm diameter.

Material composition was characterized from solution analysis of acid digested particles in *aqua regia* (3:1 v/v mixture of 37% HCl and 70% v/v HNO_3) for 2 h. All solutions were diluted in ultrapure water prior to analysis with inductively coupled plasma-optical emission spectroscopy (ICP-OES, Perkin Elmer Optima 2000). All standards were prepared in a similar acid-based matrix and was purchased as certified reference materials from Sigma Aldrich. The ion concentrations were measured using three analytical replicates and ratios of the elements were used to calculate the ultimate stoichiometries. The ICP-OES measurements indicated that the synthesized materials had the following stoichiometries: $Li_{0.27}Ni_{0.33}Mn_{0.34}Co_{0.33}O_2$ (33% Mn NMC), $Li_{0.61}Ni_{0.23}Mn_{0.55}Co_{0.22}O_2$ (55% Mn NMC) and $Li_{0.52}Ni_{0.14}Mn_{0.72}Co_{0.14}O_2$ (72% Mn NMC).

Crystal phase of the materials were characterized using powder X-ray diffraction (P-XRD). The synthesized powders were each deposited onto a SiO_2 zero-diffraction plate (MTI Corp) and then flatten down gently using a spatula to obtain an even and smooth surface of powder. To prevent loss of material during this characterization step, no other attempts were made to lower the background coming from the degree of evenness in the deposition. A Bruker D8 Advance P-XRD with a Cu-Kα source was used. The resulting reflections characterized were roughly indexed to the $R\bar{3}m$ space group as previously reported is the crystal phase for these lithium intercalation materials.[22,23] The powder XRD spectrum for $Li_{0.27}Ni_{0.33}Mn_{0.34}Co_{0.33}O_2$ (NMC 111) can be seen in Figure S1 while the P-XRD spectrum for the Mn-rich NMCs can be found in previously published work.[16]

Morphology of the synthesized materials was characterized using scanning electron microscopy (SEM, Leo Supra55 VP instrument, standard In-Lens detector at 1 kV incident electron energy). Each sample was prepared via dropcasting (methanolic solution of powder) onto boron-doped Si wafers. A large field of view containing clusters of particles was selected for each particle type to show overall morphology of a large number of particles. Representative SEM images of the material used in this study are shown in Figure S2.

Dissolution studies with ICP-OES

To characterize the concentration of ions leached from NMC-111 in bacterial growth medium, suspensions of 5 and 50 mg/L NMC-111 were prepared in triplicate and magnetically stirred at 37 °C to mimic the biological exposure of *B. subtilis* to NMC-111. At 48h, the aqueous phase was isolated using centrifugation (4696x*g* for 20 min) followed by additional ultracentrifugation of the resulting supernatant (288,000x*g* for 2 h, Beckman Coulter Optima Ultracentrifuge, SW-41 Ti Rotor). Malvern Zetasizer NanoZS dynamic light scattering instrument was used to assess effectiveness of sedimentation of particles to ensure no particles was present in the supernatant. The concentrations of released ions in the supernatants were then analyzed using ICP-OES.

Bacterial culture and nanoparticle exposure

B. subtilis SB491 was purchased from the Bacillus Genetic Stock Center (Columbus, OH). Frozen bacterial stock was inoculated on a lysogeny broth (LB) agar plate at 37 °C overnight. A colony was then suspended in a minimal growth medium (11.6 mM NaCl, 4.0 mM KCl, 1.4 mM $MgCl_2$, 2.8 mM Na_2SO_4, 2.8 mM NH_4Cl, 88.1 µM Na_2HPO_4, 50.5 µM $CaCl_2$, 10 mM HEPES, and 10 mM dextrose) to reach stationary phase with an absorbance range of 0.15~0.2 at 600 nm (OD_{600}) in a visible spectrometer (SpectroVis® Plus, Vernier Software and Technology) before exposure to nanoparticle suspensions.

To prepare a nanoparticle stock solution, the NMC cathode material was suspended in the growth medium, and sonicated for 10 minutes at 70 W. Bacterial culture at stationary phase was then diluted to OD_{600} of 0.02 into fresh media containing

NMC suspension or ionic counterparts. The cultures were incubated at 37 °C to grow.

***B. subtilis* cell growth and O_2 uptake**

Bacterial growth in the presence of NMC or ions was assessed in a 96-well plate. Stationary phase bacterial culture in minimal media was diluted 1:1 (v/v) into NMC suspension or ionic solutions in individual wells. The plate was then incubated at 37 °C in a plate reader (Synergy 2 Multi-Mode Reader, BioTek, Winooski, VT), and the absorbance at 630 nm was recorded at every 1 hour intervals for 24 hours.

Bacterial respiration upon exposure to the battery material was assessed by monitoring O_2 uptake of the cells in a 16-vessel respirometer system as reported earlier (Respirometry Systems and Applications, Inc., Springdale, AR).[8,24] In each 125-mL isobaric vessels, 100-mL of *B. subtilis* culture was grown in growth media containing the battery material or corresponding amounts of dissolved ions. CO_2 from bacterial respiration was removed by a capsule of 1 M KOH in the vessel, while O_2 delivered to the vessel was monitored with a pressure sensor.

Single cell electrophoresis for DNA damage of *B. subtilis*

Single cell electrophoresis on nanoparticle or metal ion-treated *B. subtilis* cells was conducted following the protocols published earlier with modifications.[25,26] Ten microliter of the nanoparticle-treated cell suspension was mixed with 100 µL of 0.5% low-melting agarose (LMA) solution. Immediately after mixing, 40 µL of the suspension was pipetted onto a well of a Comet assay microscope slide (Travigen®) and spread evenly. The gel was allowed to solidify at 4 °C. A lysozyme-LMA layer containing 0.5% of lysozyme solution was placed on top of the first layer of gel, and was incubated at 4 °C to solidify. The assembled slide was then transferred to 37 °C incubator for 30 minutes. Each slide was then immersed in a lysing solution (2.5 M NaCl, 100.0 mM EDTA, 10.0 mM Tris-HCl, and 1% sodium N-lauryl sarcosine, 1% Triton® X-100, pH 10.0) at room temperature for 1 hour in the dark, followed by a 2 hour incubation in an enzyme digestion solution (2.5 M NaCl, 10.0 mM EDTA, 10.0 mM Tris-HCl, and 0.5 mg/mL proteinase K, pH 7.4) at 37 °C. Electrophoresis was performed in a neutral electrophoresis buffer (sodium acetate and Tris, pH 9.0) at 12 V for 30 minutes. The slide was then washed and dehydrated in a 1.0 M ammonium acetate in ethanol followed by absolute ethanol, and was left at room temperature to dry in the dark. Freshly prepared DMSO solution (5% DMSO and 10 mM NaH_2PO_4) was used to rehydrate the stack of microgel. The DNA was then stained with 20.0 µL of 1.0 µM YOYO-1 in 5% DMSO. Slide was left to air dry in the dark for 5 minutes before coverslips were placed. Each stack of microgel was imaged under a fluorescent microscope (100x, λ_{ex} = 491 nm, λ_{em} = 509 nm). ImageJ software was used to analyze the DNA tail lengths.

***B. subtilis* spore and surfactin secretion analysis**

Positive control for spore formation was carried out by growing *B. subtilis* in Difco Sporulation Media (DSM) (8 g Difco® bacto nutrient broth, 1 g KCl, and 0.12 g $MgSO_4 \cdot 7H_2O$ in 1-L MQ water, pH 7.6). After autoclaving and prior to use, 1.0-mL each of sterile solutions of 1.0 M $Ca(NO_3)_2$, 0.010 M $MnCl_2$, and 1.0 mM $FeSO_4$ were added to the media. *B. subtilis* colonies from an LB agar plate were inoculated in DSM and incubated at 37 °C and 250xg for approximately 48 hours.

To image spores in both spore-positive control and nanoparticle-treated cultures, optical microscopy with differential staining method was used according to an established method.[27] Once cells were harvested by centrifugation at 750xg for 10 minutes, and resuspending in ultrapure water, a 10-µL aliquot was placed on glass slide, and allowed to air dry. *B. subtilis* on microscope slide was then heat fixed and covered with a piece of filter paper flooded with 5% malachite green, and placed above boiling water for 5 minutes. After malachite green was rinsed off with water, the *B. subtilis* cells were counterstained with 0.25% safranin O for 90 seconds, rinsed with water, and allowed to air dry. Samples were imaged under oil immersion lens at 100X. With this method, spores were stained greenish blue, and vegetative cells were red. Bright-field microscopic images were then analyzed manually by counting the total number of cells and the number of spores, and a spore-to-cell ratio was reported.

Surfactin secretion from *B. subtilis* in high Mn^{2+} environment was investigated by LCMS (UHD Accurate-Mass Q-TOF, Agilent 6540) from *B. subtilis* cultures grown in different growth media at 37 °C for 48 hours. The negative control cultures were grown in LB media (2.5 g LB in 100 mL ultrapure water). For a high Mn^{2+} growth medium, LB doped with 0.072 mg/L Mn^{2+} was used. Five-microliter samples of supernatants from bacterial cultures after centrifugation (3,220xg, 4 °C, 10 min) were separated on a reverse phase C18 column (Agilent, Eclipse Plus, 2.1 x 50 mm, 1.8 µm), and detected by electrospray ionization (positive ion mode, gas temp 325 °C, source/fragmentor 100 V, capillary voltage 4000 V, 100-1700 m/z). Samples were separated with an isocratic elution of 60% solvent A (95:5 H_2O:ACN with 0.1% ammonium acetate) at 0.40 mL/min for 1 min followed by a linear gradient of 40-70% solvent B (95:5 ACN:H_2O with 0.1% ammonium acetate) over 15 minutes, then an linear gradient of 70-100% B for 2 minutes, then an isocratic elution at 100% B for 2 min. Identity of surfactin was confirmed by comparing the exact mass, retention time, and fragmentation spectra (35 V) to a purchased surfactin standard (Sigma Aldrich). Sample mass spectra of surfactin are shown in Figure S3. The data was analyzed with the Agilent Mass Hunter Quantitative Analysis suite. Extracted ion chromatograms were integrated and the area of the peak was normalized to the OD_{600} value of each culture.

Results and Discussion

Dissolution and solution speciation analysis

An earlier study evaluating the toxicity mechanism of NMC to a Gram-negative model bacterium, *Shewanella oneidensis* has indicated that the ion dissolution from NMC, in particular, the dissolved Ni and Co ions, are largely responsible for the toxicity

to the bacterium, and the dissolution reached equilibrium within an hour.[8] Therefore, it is important to characterize the dissolution behavior of NMC in *B. subtilis* growth media. ICP-OES analysis of the supernatant from 5 mg/L NMC suspension, shown in Figure 1(a), indicate that significantly higher concentrations of Li and Ni ions were released compared to those of Mn and Co, , in agreement with the incongruent dissolution of such MO_2 nanosheet framework reported earlier. [Hang 2016, Bennett 2017]. Molar concentration analysis of the species also indicates that a higher percentage of Ni (26.3%) was dissolved from the NMC bulk material, in comparison to Mn (3.8%) and Co (9.0%).

To better understand the solution chemistry of NMC dissolution in *B. subtilis* growth media, we performed a solution speciation simulation using the Visual MINTEQ (https://vminteq.lwr.kth.se/), a chemical solution equilibrium model. Fig 1(b) shows the major species present (> 1%) as a percentage of each dissolved ions from Fig 1(a) in the given minimal medium composition for *B. subtilis*. The patterned bars indicate the free ion form of each metal. Therefore, the simulation shows that for all four elements, more than 85% of each stayed in solution as free 2+ ions.

Impact of NMC to *B. subtilis* Growth and Respiration

The impact of NMC nanomaterial on *B. subtilis* was investigated with respirometry and growth curves. Respiration, a functional parameter, assesses metabolic activity of bacterial cultures, probes a different end-point compared to the growth assay examining optical turbidity resulted from changes in biomass. Respirometry monitors the oxygen uptake by bacterial cultures in pressure-controlled vessels for an extended period of time. [8,16,24] In the absence of nanomaterial, the respiration profile (black symbol in Fig 2) of *B. subtilis* culture resembles that of a healthy growth curve, because the amount of O_2 consumed by the bacterial culture is proportional to the number of metabolically active cells. However, in the presence of 5 mg/L NMC nanoparticle, the respirometry curve is significantly altered. Instead of a distinctive lag-exponential-stationary phase profile, the respirometry curve is rather flat with gradual increase in O_2 consumption. In contrast to the delayed respiration response in *S. oneidensis* by 5 mg/L NMC, where the cell culture eventually still reached a similar level of O_2 uptake level[8], when incubated with NMC, *B. subtilis* never reached the same level of O_2 consumption, even when monitored beyond 48 hours. This observation indicates that *B. subtilis* and *S. oneidensis* have different responses to NMC toxicity. At the same dosage level, while NMC resulted in delays in oxygen uptake during *S. oneidensis* growth, it severely suppressed this metabolic activity in *B. subtilis*.

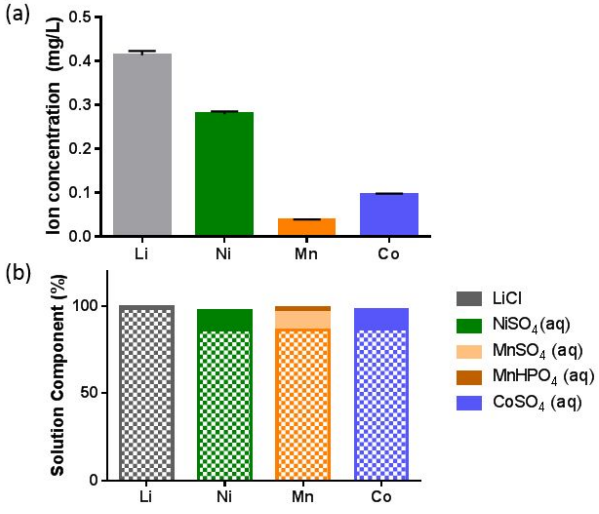

Figure 1. (a) Dissolved ion concentrations from 5 mg/L NMC suspension in B. subtilis growth minimal media over 48 hours by ICP-OES analysis (error bars are standard deviation, n = 3); (b) Speciation simulation of solution species (patterned bars indicating free ions).

To confirm the observed suppression in respiration, growth curves of *B. subtilis* in the presence of 5 mg/L NMC were also collected at OD_{630}. We note that the presence of NMC as a colloid suspension could introduce optical interference to OD measurements, and the extent of interference was not additive in the presence of bacterial cells. Therefore, simple background subtraction of NMC suspension may not have fully corrected for this background. Figure 2(b) shows that, in agreement with respirometry results, 5 mg/L NMC in growth media hinders the growth of *B. subtilis*. The cultures are unable to recover to the same optical density as the control cultures.

Since previous studies have demonstrated that dissolved metal ions from NMC, especially Ni^{2+} and Co^{2+}, are toxic to *S. oneidensis*, we investigate if this finding is also applicable to *B. subtilis*. Figure 3 shows the responses of both *B. subtilis* growth and respiration to 5 mg/L NMC suspension and the corresponding Ni and Co ions released from 5 mg/L NMC according to the ICP-OES measurements in Fig 1(a). Since the growth curves obtained from optical turbidity of cell cultures in the presence of Li^+ and Mn^{2+} ions show minimal impact to *B. subtilis* as predicted (Figure S4), we focused mainly on the impact of Ni^{2+} and Co^{2+} ions in this study. In the presence of given amounts of Ni^{2+} and Co^{2+}, we evaluated bacterial respiration shown in Fig 3(a). The oxygen uptake curves reveal that the impact on bacterial respiration by Co^{2+} is less significant than that of Ni^{2+}. In the presence of 0.096 mg/L Co^{2+}, the respirometry profile of *B. subtilis* showed a delayed lag-phase with recovery beyond 30 hours. However, Ni^{2+} significantly suppressed the respiration with minimal recovery. Remarkably,

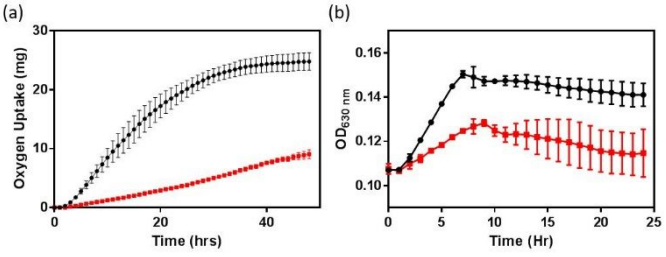

Figure 2. Impacts on bacterial respiration (a) and growth (b) of B. subtilis in minimal growth media without (black) and with 5 mg/L NMC (red). Error bars represent standard deviation from three replicates.

the O_2 uptake curve of *B. subtilis* with Ni^{2+} in growth medium completely overlapped with that in the presence of 5 mg/L NMC. This result suggests that Ni ion released from NMC is the major contributor to the hindered respiration of *B. subtilis* by NMC. The combined impact of Ni^{2+} and Co^{2+} ions on bacterial respiration also traces those of the respiration curves in NMC and Ni^{2+} ion-containing media (plotted separately for clarity in Figure S5).

Optical turbidity measurements of *B. subtilis* cultures in the presence of Ni^{2+} and Co^{2+} ions, respectively, have also both resulted in reduced growth, as shown in Fig 3(b). Due to the optical interference by NMC colloidal suspension mentioned previously, no direct comparisons of growth curves was made between those in the presence of ions with that of the NMC suspension (i.e. no brown trace in Fig 3(b)). However, comparing the growth curves of Ni^{2+} and Co^{2+}-containing media, we observe that Co^{2+} ion affects growth more severely than Ni^{2+} ion, opposite to those observed in respirometry measurements. Results in Fig. 3 demonstrate the subtle differences in these assays. When we examine the effect of both Ni^{2+} and Co^{2+} ions, the growth curves fall in between those from the two individual ions-containing media, with no statistical differences in OD readings at the end of a 24-hour growth period.

Overall, material characterizations and ion dissolution studies indicate the incongruent dissolution to produce Li, Ni and Co ions in *B. subtilis* growth media, similar to previously reported.[8,28] However, media constituents (lactate in case of *S. oneidensis* media vs. dextrose in *B. subtilis* media) dictate that the dissolved ions mainly stay in their free ion form, which impacts *B. subtilis* growth and respiration continuously.

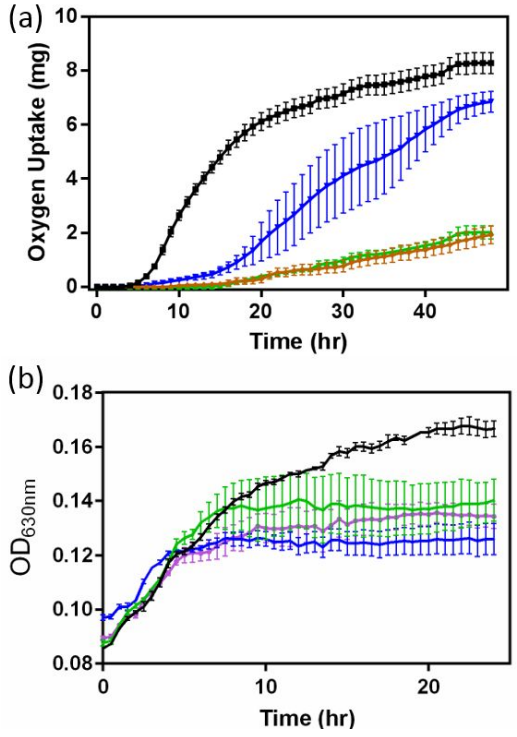

Figure 3. Response of B. subtilis cultures to NMC and selected ions dissolved from NMC monitored by oxygen uptake (a) and optical density (b) in minimal growth medium (black), or media containing 0.279 mg/L Ni^{2+} (green), 0.096 mg/L Co^{2+} (blue), a combination of Ni^{2+} and Co^{2+} (purple) and 5.0 mg/L NMC (brown). Chloride salts were used for all the ions. Error bars represent standard error of means from at least three replicates.

B. subtilis DNA damage by NMC

Previous studies have suggested that metal toxicity in bacterial species could be through the displacement of essential metal from their binding sites or through interactions with nucleic acids and proteins by altering their conformations.[18] In addition, because cobalt is in a 3+ oxidation state in NMC, dissolution leads to ions in valence states that can induce oxidation of water or OH^-, producing reactive oxygen species such as hydroxyl radicals.[8] A solution ROS assay using a fluorescence probe also showed the formation of ROS species from NMC nanosheet suspensions.[16] Therefore, we hypothesize that solution suspensions of NMC may induce oxidative stress and DNA damage in *B. subtilis* as a mechanism of toxicity.

Bacterial DNA damage induced by the presence of the NMC material was investigated with single cell gel electrophoresis, also known as the comet assay. The comet assay, a term originated from the comet-like tails of the fragmented DNA in single cells, is a highly sensitive tool that provides a direct visualization of lesions in DNA breakage and allows for quantification by comparing the damaged DNA tail lengths. [29,30] Its application in genotoxicity studies of nanomaterials, primarily in mammalian cells, has been demonstrated recently.[31,32] The method has recently been adapted to bacterial cells[25,33,34], yielding DNA tails less resemblant of comets, but more of bolts of lightning. Yet its application in understanding genotoxicity induced by nanomaterials in bacterial species is rare.[35] In our study, DNA tail lengths from individual NMC-exposed cells were compared to those of unexposed cells. Sample fluorescence microscopy images are shown in Figure S6, where the longer the DNA tails, the more severe the DNA damage.

Figure 4(a) shows the results of DNA tail length comparisons from cells exposed to 0, 5 mg/L NMC suspension, as well as to the corresponding amounts of dissolved Ni^{2+} and Co^{2+} ions after 48 hours of growth. Control samples resulted in an average tail length of 5.3 ± 0.4 µm with many intact cells in fluorescence images. In contrast, 5 mg/L NMC-exposed *B. subtilis* cells had averages tail lengths of 18.2 ± 0.8 µm. Statistical analysis reveals that compared to the control group, NMC exposed populations had significant DNA damage (denoted by letter “a” and “b”).

Results from respirometry and growth curves in Fig 3 suggest that Ni^{2+} and Co^{2+} ions are key contributors to NMC toxicity to *B. subtilis*. The comet assay results in Fig. 4 reveal that the extent of DNA damage induced by the combination of Ni^{2+} and Co^{2+} ions recapitulates that of NMC. In comparison, cells from Ni^{2+} and Co^{2+} ion-containing media resulted in average DNA tail lengths of 10 ± 1 µm and 11.3 ± 0.4 µm, respectively. The two groups yielded no statistical difference with an unpaired *t*-test

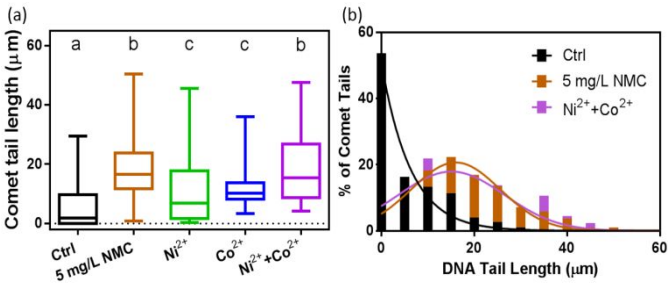

Figure 4. DNA comet tail length analysis from the comet assay showing DNA damages in *B. subtilis* when exposed to 5 mg/L of NMC (brown), 0.279 mg/L Ni^{2+} (green), 0.096 mg/L Co^{2+} (blue), and both Ni^{2+} and Co^{2+} (purple) in box-and-whisker plot (a) and histograms (b). Data sets with different letters (a, b, and c) differ statistically ($p < 0.05$).

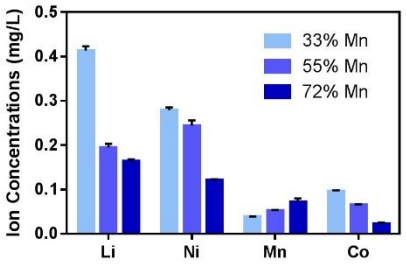

Figure 5. Ionic concentrations of species in B. subtilis minimal growth media dissolved from NMC materials containing varying amount of Mn: 33% (light blue), 56% (medium blue), and 70% (dark blue) quantified by ICP-MS.

(both denoted by letter "c"). We observe that the DNA damage was more heterogeneous at the single cell level with Ni^{2+} ions, compared to that from Co^{2+} ions, demonstrated by the standard deviations of tail lengths. In addition, Ni^{2+} and Co^{2+} ions individually, although both induced DNA damage when compared to the control group, resulted in less DNA damage than that from 5 mg/L NMC (denoted by letters "a" and "c"). These results reveal that the amount of Ni^{2+} and Co^{2+} ions dissolved from 5 mg/L NMC caused significant DNA damage to *B. subtilis*, yet the extent of the damage is less than that with NMC nanoparticles. Remarkably, however, when both ions are present, shown in the purple bar in Fig 4(a), the resulting average of DNA tail lengths is 19 ± 1 μm, statistically identical to that of the 5 mg/L NMC (denoted by letter "b"). This comparison is also shown more clearly when replotted in histogram in Fig 4(b).

Ni^{2+} has been linked to genotoxicity to both mammalian and bacterial cells by inducing oxidative DNA damage and interfering with DNA repair mechanisms in the presence of additional DNA damaging agents.[36] A molecular-level genotoxicity study in *E. coli* has found that Ni(II) complexed to the tripeptide Gly-Gly-His in combination with hydrogen peroxide induce mutations *in vitro* on single-stranded DNA typical for damage by oxygen free radicals.[37] Co^{2+} has also been reported to be mutagenic in certain bacterial strains.[38] Our finding from DNA damage analysis reveals an important mechanism of toxicity by NMC to *B. subtilis*. Although ROS generation leading to DNA damage is often considered as a mode of nanotoxicity to bacteria[39], only a few studies have examined DNA damage directly.[35,40,41] In contrast to the studies that focus on intracellular ROS species, which are often transient, the comet assay probes an end-point of resulting DNA damage with high sensitivity at the single cell level.

Mn-enriched NMC

An earlier study has reported that the Ni^{2+} and Co^{2+} ions released from nanoscale NMC materials have been the main contributors to NMC toxicity toward a model Gram-negative bacterium, *S. oneidensis*.[8] In an effort to remediate the adverse biological impact of NMC, several NMC materials with reduced Ni and Co content were synthesized, and their biological impact was tested against *S. oneidensis*.[16] In that work, increasing the Mn fraction (with concurrent reduction in Ni and Co content) decreased the amount of Ni and Co ions released into solution, and that this reduction mitigated the impact on *S. oneidensis* respiration. Therefore, we are interested in examining the toxicity of these Mn-enriched NMC nanomaterials on the Gram-positive model, *B. subtilis*, and to evaluate if the redesign is a viable approach across multiple biological species. We note that although the Mn-enriched NMC material studied here have not been tested in commercial batteries, a variety of NMC compositions are commercially available[7,11], which suggests the variabilities in this class of material that have comparable performance. Two Mn-enriched NMC materials were evaluated in this study, $Li_{0.61}Ni_{0.23}Mn_{0.55}Co_{0.22}O_2$ (55% Mn) and $Li_{0.52}Ni_{0.14}Mn_{0.72}Co_{0.14}O_2$ (72% Mn). These materials were compared to that of the NMC-111 (33% Mn) for their biological impact.

Guided by the hypothesis that the released ions, especially Ni^{2+} and Co^{2+}, in growth media are the key contributors to toxicity to *B. subtilis*, we analyzed the ionic species present in minimal media with 5 mg/L Mn-enriched NMC nanosheets after 48 hours by ICP-OES. Fig 5 shows a comparison of dissolved ions from the three NMC variants for each of the four metals. Distinctively, Li, Ni, and Co ions present in the media decreased as the Mn fraction increases from 33% to 72% in the material lattice, while the corresponding amounts of Mn ion increased. This trend echoes that observed in the *S. oneidensis* growth medium.[16]

Given the impact of Ni^{2+} and Co^{2+} on growth and respiration of *B. subtilis* (Fig 3), we hypothesize that the decrease in their concentrations in media with Mn-enriched NMC variants would lead to reduced toxicity of these materials to *B. subtilis*. The biological impact of the Mn-enriched NMC to *B. subtilis* was assessed again with respirometry, and compared to that of NMC-111 (33% Mn). Fig 6 shows oxygen uptake over a 48-hour period by *B. subtilis* cultures in pressure-regulated vessels with 5 mg/L of each NMC variants. We observe that, while 33% Mn severely suppressed oxygen uptake by bacterial cultures, the cellular respiration profiles from cultures incubated with either 55%, or 72% Mn NMC variants strongly resemble that of the control culture. The final levels of oxygen uptake at 48 hours follow the trend of 33% Mn < 55% Mn ≤ 72% Mn < no NMC, with no statistical significance between 55% and 72% Mn using a *t*-

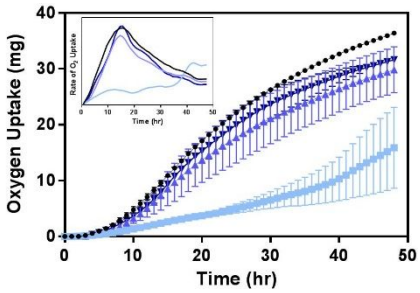

Figure 6. Oxygen uptake of cellular respiration by B. subtilis upon exposure to NMC materials containing various amount of Mn: 33% (light blue), 56% (medium blue), and 70% (dark blue). Inset: First derivative of the respirometry curves to indicate rate of oxygen uptake.

test. We also note that the rates of oxygen uptake by cultures incubated with NMC were nearly identical among control samples and those with either 55% or 72% Mn NMC, as shown in the first derivative plot of the respirometry curves in the inset. These results support the hypothesis that Mn-enrichment in NMC that resulted in lower nickel and cobalt fractions in the material lattice reduced Ni^{2+} and Co^{2+} ion release in aqueous suspension, and hence successfully mitigated toxicity to *B. subtilis*.

Additional Biological Impact of Mn-enrichment to *B. subtilis*

Previous studies on the impact of metal ions to bacterial species have revealed that Mn^{2+} is an essential component in growth environment of *B. subtilis*, affecting cellular activities and pathways of various processes, such as mobility, endospore and biofilm formation, and antibiotic production.[42,43] Therefore, to thoroughly evaluate any additional unintended impact of NMC redesign, we examine *B. subtilis* sporulation and surfactin production activities as biological indicators.

Sporulation is an adaptive response to environmental changes for certain bacterial species, such as those in the genera of *Bacillus*.[44–46] In the sporulation process, vegetative cells undergo an asymmetric division, where chromosomes are copied and protected by a special cortex. Endospores are usually formed in harsh environmental conditions, such as heat, radiation, or nutrient depletion. The mechanism allows cells to re-germinate with the conserved genetic information when the growth environment restores.[44,47] Mn^{2+} has been identified as an essential mineral for endospore formation[48] by controlling the proper functions of phosphoglycerate phosphomutase (PGA-mutase), an enzyme needed for optimal sporulation in growth media.[49,50]

We examined bacterial cultures after 48-hour incubation in growth media containing Mn-enriched NMC nanomaterials using differential staining to identify spores versus vegetative cells under a bright field optical microscope. Malachite Green, retained by the spore coat stains the spores green, while Gram stain, Safanine stains the vegetative cells red. As shown in Fig 7, image analysis reveals that there is an increasing trend from 33% to 70% Mn-enriched NMC samples in the spore-to-cell ratios. Cultures exposed to growth media containing NMC with

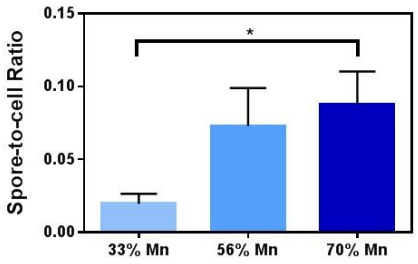

Figure 7. Spore-to-cell ratio from microscopy image analysis upon cells exposed to 5 mg/L of Mn-enriched varieties of NMC.

70% Mn resulted in the most endospores per view, yet the large majority of cells are still in the vegetative state. The spore-to-cell ratio from these images shows a significant difference from that from the 33% Mn samples. The results confirm that the increased Mn in NMC nanosheets which led to increased Mn^{2+} concentration in media indeed induces sporulation in *B. subtilis*.

Surfactin is one of the well-known biosurfactant lipopeptides secreted by *B. subtilis* and has potent antimicrobial activities.[51] Certain metal cations, especially manganese and iron, have been identified to spur its production and have been applied in industrial bioreactors to induce the biosynthesis of surfactin.[52] We hypothesize that the redesigned Mn-enriched NMC may also induce surfactin production in *B. subtilis* cultures. Therefore, surfactin secretion was compared by growing *B. subtilis* cultures in 0.072 mg/L Mn^{2+} containing medium, corresponding to the amount of Mn^{2+} dissolved from 5 mg/L of the 72% Mn-enriched NMC to avoid potential interference of NMC nanosheets in the LCMS analysis. A feature was detected at m/z 1036.7[51], corresponding to a C_{15} isoform of surfactin, which was then compared to unexposed cultures. Figure 8 shows that Mn doping induces 8.5-times more surfactin production from *B. subtilis*. Surfactin is used as a signalling molecule, which can induce biofilm formation[53], and has a moderate ability to chelate metal ions.[54] Therefore, surfactin secretion on its own has been suggested as a defense mechanism against an increase in metal concentrations, especially in Mn^{2+}, as observed here.

The sporulation and surfactin production studies highlight the ecological sensitivity to material compositions. In this case, the observed impacts are in agreement with that predicted from ion

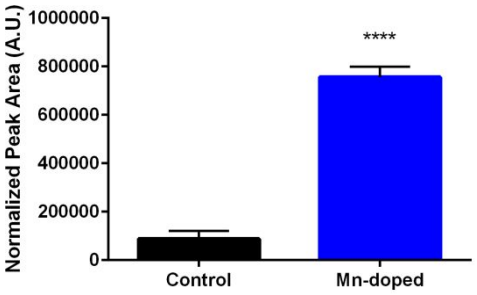

Figure 8. Surfactin production from B. subtilis cultures grown in media with and without 0.072 mg/L Mn^{2+} (unpaired t-test, $p < 0.0001$).

dissolution studies. These observations also suggest the needs for evaluating the environmental impact of nanomaterial with mixed cultures over longer periods of time to examine the long-term impact of nanomaterial on the microbial communities.

Conclusions

In this study, we expand our understanding of the biological impact of an emerging class of nanomaterial as potential environmental stressors, complex metal oxides, NMC, to a Gram-positive model bacterium, *B. subtilis*. Although the environmental impact, especially to the microbial communities, of nanomaterials composed of simple metal oxides have been more extensively studied[21], these new materials pose more complex challenges where multiple factors in determining environmental impact need to be considered. Together with our earlier publications in this area, the current study demonstrates that the incongruent dissolution behavior of the material, as well as solution constituents are important factors when dissolved ions are major contributors to biological impact. In addition, this is our first step towards a mechanistic understanding of genotoxicity induced by complex metal oxides where transition metal oxidative states may pose additional oxidative stress in an organism as a means for DNA damage. This preliminary study calls for a more in-depth investigation of the mechanism of intracellular ROS generation and chemical evidence of DNA damage. Lastly, our effort in material redesign, which has successfully reduced toxicity to another model bacterium, *S. oneidensis*, has been shown to also be effective in mitigating toxicity to *B. subtilis*. Yet, additional biological consequences, such as increased sporulation and antibiotic secretion have also been observed. Although thorough material redesign also needs to take functionality into consideration, this proof-of-concept effort demonstrates the importance of a fundamental understanding of biological impacts from all aspects of material redesign.

Conflicts of interest

There are no conflicts to declare.

Acknowledgements

This work was supported by the National Science Foundation under the Center for Sustainable Nanotechnology (CSN), CHE-1503408. The CSN is part of the Centers for Chemical Innovation Program. S.L.M. acknowledges the NIH Chemistry−Biology Interface Training Grant 5T32GM008700-18. TP acknowledges the Lindstrom Research Fund through Augsburg University. The authors gratefully acknowledge Dr. Michael P. Schwartz for helpful discussion.

References

(1) Patel, P. Improving the Lithium-Ion Battery. *ACS Cent. Sci.* **2015**, *1* (4), 161–162.

(2) Etacheri, V.; Marom, R.; Elazari, R.; Salitra, G.; Aurbach, D. Challenges in the Development of Advanced Li-Ion Batteries: A Review. *Energy Environ. Sci.* **2011**, *4* (9), 3243.

(3) Goodenough, J. B.; Park, K.-S. The Li-Ion Rechargeable Battery: A Perspective. *J. Am. Chem. Soc.* **2013**, *135* (4), 1167–1176.

(4) Goodenough, J. B.; Kim, Y. Challenges for Rechargeable Li Batteries. *Chem. Mater.* **2010**, *22* (3), 587–603.

(5) Wang, Y.; Cao, G. Developments in Nanostructured Cathode Materials for High-Performance Lithium-Ion Batteries. *Adv. Mater.* **2008**, *20* (12), 2251–2269.

(6) Meng, J.; Niu, C.; Liu, X.; Liu, Z.; Chen, H.; Wang, X.; Li, J.; Chen, W.; Guo, X.; Mai, L. Interface-Modulated Approach toward Multilevel Metal Oxide Nanotubes for Lithium-Ion Batteries and Oxygen Reduction Reaction. *Nano Res.* **2016**, *9* (8), 2445–2457.

(7) Andre, D.; Kim, S.-J.; Lamp, P.; Lux, S. F.; Maglia, F.; Paschos, O.; Stiaszny, B. Future Generations of Cathode Materials: An Automotive Industry Perspective. *J. Mater. Chem. A* **2015**, *3* (13), 6709–6732.

(8) Hang, M. N.; Gunsolus, I. L.; Wayland, H.; Melby, E. S.; Mensch, A. C.; Hurley, K. R.; Pedersen, J. A.; Haynes, C. L.; Hamers, R. J. Impact of Nanoscale Lithium Nickel Manganese Cobalt Oxide (NMC) on the Bacterium textitShewanella Oneidensis MR-1. *Chem. Mater.* **2016**, *28* (4), 1092–1100.

(9) Sun, Y.; Liu, N.; Cui, Y. Promises and Challenges of Nanomaterials for Lithium-Based Rechargeable Batteries. *Nat. Energy* **2016**, *1* (7), 16071.

(10) Martha, S. K.; Sclar, H.; Szmuk Framowitz, Z.; Kovacheva, D.; Saliyski, N.; Gofer, Y.; Sharon, P.; Golik, E.; Markovsky, B.; Aurbach, D. A Comparative Study of Electrodes Comprising Nanometric and Submicron Particles of LiNi0.50Mn0.50O2, LiNi0.33Mn0.33Co0.33O2, and LiNi0.40Mn0.40Co0.20O2 Layered Compounds. *J. Power Sources* **2009**, *189* (1), 248–255.

(11) Olivetti, E. A.; Ceder, G.; Gaustad, G. G.; Fu, X. Lithium-Ion Battery Supply Chain Considerations: Analysis of Potential Bottlenecks in Critical Metals. *Joule* **2017**, *1* (2), 229–243.

(12) Dewulf, J.; der Vorst, G.; Denturck, K.; Van Langenhove, H.; Ghyoot, W.; Tytgat, J.; Vandeputte, K. Recycling Rechargeable Lithium Ion Batteries: Critical Analysis of Natural Resource Savings. *Resour. Conserv. Recycl.* **2010**, *54* (4), 229–234.

(13) Notter, D. A.; Gauch, M.; Widmer, R.; Wäger, P.; Stamp, A.; Zah, R.; Althaus, H.-J. Contribution of Li-Ion Batteries to the Environmental Impact of Electric Vehicles. *Environ. Sci. Technol.* **2010**, *44* (17), 6550–6556.

(14) Larcher, D.; Tarascon, J.-M. Towards Greener and More Sustainable Batteries for Electrical Energy Storage. *Nat. Chem.* **2014**, *7* (1), 19–29.

(15) Doğangün, M.; Hang, M. N.; Troiano, J. M.; McGeachy, A. C.; Melby, E. S.; Pedersen, J. A.; Hamers, R. J.; Geiger, F. M. Alteration of Membrane Compositional Asymmetry by LiCoO _textrm2 Nanosheets. *ACS Nano* **2015**, *9* (9), 8755–8765.

(16) Gunsolus, I. L.; Hang, M. N.; Hudson-Smith, N. V; Buchman, J. T.; Bennett, J. W.; Conroy, D.; Mason, S. E.; Hamers, R. J.; Haynes, C. L. Influence of Nickel Manganese Cobalt Oxide Nanoparticle Composition on Toxicity toward Shewanella Oneidensis MR-1: Redesigning for Reduced Biological Impact. *Environ. Sci. Nano* **2017**, *4* (3), 636–646.

(17) Bozich, J.; Hang, M.; Hamers, R.; Klaper, R. Core Chemistry Influences the Toxicity of Multicomponent Metal Oxide Nanomaterials, Lithium Nickel Manganese Cobalt Oxide, and Lithium Cobalt Oxide to textitDaphnia Magna: Battery Material Core Chemistry Influences Aquatic Toxicology. *Environ. Toxicol. Chem.* **2017**.

(18) Bruins, M. R.; Kapil, S.; Oehme, F. W. Microbial Resistance to Metals in the Environment. *Ecotoxicol. Environ. Saf.* **2000**, *45* (3), 198–207.

(19) Malik, A. Metal Bioremediation through Growing Cells. *Environ. Int.* **2004**, *30* (2), 261–278.

(20) Valentine, N. B.; Bolton, H.; Kingsley, M. T.; Drake, G. R.; Balkwill, D. L.; Plymale, A. E. Biosorption of Cadmium, Cobalt, Nickel, and Strontium by aBacillus Simplex Strain Isolated from the Vadose Zone. *J. Ind. Microbiol.* **1996**, *16* (3), 189–196.

(21) McKee, M. S.; Filser, J. Impacts of Metal-Based Engineered Nanomaterials on Soil Communities. *Environ. Sci. Nano* **2016**, *3* (3), 506–533.

(22) Okubo, M.; Hosono, E.; Kim, J.; Enomoto, M.; Kojima, N.; Kudo, T.; Zhou, H.; Honma, I. Nanosize Effect on High-Rate Li-Ion Intercalation in LiCoO2 Electrode. *J. Am. Chem. Soc.* **2007**, *129* (23), 7444–7452.

(23) Lu, Z.; MacNeil, D. D.; Dahn, J. R. Layered Li[Ni[Sub x]Co[Sub 1−2x]Mn[Sub x]]O[Sub 2] Cathode Materials for Lithium-Ion Batteries. *Electrochem. Solid-State Lett.* **2001**, *4* (12), A200.

(24) Feng, Z. V.; Gunsolus, I. L.; Qiu, T. A.; Hurley, K. R.; Nyberg, L. H.; Frew, H.; Johnson, K. P.; Vartanian, A. M.; Jacob, L. M.; Lohse, S. E.; et al. Impacts of Gold Nanoparticle Charge and Ligand Type on Surface Binding and Toxicity to Gram-Negative and Gram-Positive Bacteria. *Chem. Sci.* **2015**, *6* (9), 5186–5196.

(25) Solanky, D.; Haydel, S. E. Adaptation of the Neutral Bacterial Comet Assay to Assess Antimicrobial-Mediated DNA Double-Strand Breaks in Escherichia Coli. *J. Microbiol. Methods* **2012**, *91* (2), 257–261.

(26) Olive, P. L.; Banáth, J. P. The Comet Assay: A Method to Measure DNA Damage in Individual Cells. *Nat. Protoc.* **2006**, *1* (1), 23–29.

(27) Reynolds, J.; Moyes, R.; Breakwell, D. P. Differential Staining of Bacteria: Endospore Stain. In *Current Protocols in Microbiology*; John Wiley & Sons, Inc.: Hoboken, NJ, USA, 2009; Vol. Appendix 3, p Appendix 3J.

(28) Bennett, J. W.; Jones, D.; Huang, X.; Hamers, R. J.; Mason, S. E. Dissolution of Complex Metal Oxides from First-Principles and Thermodynamics: Cation Removal from the (001) Surface of $Li(Ni_{1/3}Mn_{1/3}Co_{1/3})O_2$. *Environ. Sci. Technol.* **2018**, *52* (10), 5792–5802.

(29) Azqueta, A.; Collins, A. R. The Essential Comet Assay: A Comprehensive Guide to Measuring DNA Damage and Repair. *Arch. Toxicol.* **2013**, *87* (6), 949–968.

(30) Liao, W.; McNutt, M. A.; Zhu, W.-G. The Comet Assay: A Sensitive Method for Detecting DNA Damage in Individual Cells. *Methods* **2009**, *48* (1), 46–53.

(31) Armand, L.; Tarantini, A.; Beal, D.; Biola-Clier, M.; Bobyk, L.; Sorieul, S.; Pernet-Gallay, K.; Marie-Desvergne, C.; Lynch, I.; Herlin-Boime, N.; et al. Long-Term Exposure of A549 Cells to Titanium Dioxide Nanoparticles Induces DNA Damage and Sensitizes Cells towards Genotoxic Agents. *Nanotoxicology* **2016**, *10* (7), 913–923.

(32) Karlsson, H. L. The Comet Assay in Nanotoxicology Research. *Anal. Bioanal. Chem.* **2010**, *398* (2), 651–666.

(33) Singh, N.; Manshian, B.; Jenkins, G. J. S.; Griffiths, S. M.; Williams, P. M.; Maffeis, T. G. G.; Wright, C. J.; Doak, S. H. NanoGenotoxicology: The DNA Damaging Potential of Engineered Nanomaterials. *Biomaterials* **2009**, *30* (23–24), 3891–3914.

(34) El-Sonbaty, S. M.; El-Hadedy, D. E. Combined Effect of Cadmium, Lead, and UV Rays on Bacillus Cereus Using Comet Assay and Oxidative Stress Parameters. *Environ. Sci. Pollut. Res.* **2015**, *22* (5), 3400–3407.

(35) Anas, A.; Jiya, J.; Rameez, M. J.; Anand, P. B.; Anantharaman, M. R.; Nair, S. Sequential Interactions of Silver-Silica Nanocomposite (Ag-SiO NC) with Cell Wall, Metabolism and Genetic Stability of textitPseudomonas Aeruginosa , a Multiple Antibiotic-Resistant Bacterium. *Lett. Appl. Microbiol.* **2013**, *56* (1), 57–62.

(36) Hartwig, A. Current Aspects in Metal Genotoxicity. *Biometals* **1995**, *8* (1).

(37) Tkeshelashvili, L. K.; Reid, T. M.; Mi-Bride, T. J.; Loe, L. A. *Nickel Induces a Signature Mutation for Oxygen Free Radical Damage1*; 1993; Vol. 53.

(38) Pagano, D. A.; Zeiger, E. Conditions for Detecting the Mutagenicity of Divalent Metals InSalmonella Typhimurium. *Environ. Mol. Mutagen.* **1992**, *19* (2), 139–146.

(39) Suresh, A. K.; Pelletier, D. A.; Doktycz, M. J. Relating Nanomaterial Properties and Microbial Toxicity. *Nanoscale* **2013**, *5* (2), 463.

(40) Hwang, E. T.; Lee, J. H.; Chae, Y. J.; Kim, Y. S.; Kim, B. C.; Sang, B.-I.; Gu, M. B. Analysis of the Toxic Mode of Action of Silver Nanoparticles Using Stress-Specific Bioluminescent Bacteria. *Small* **2008**, *4* (6), 746–750.

(41) Guo, Z.; Xue, J.; Liu, T.; Song, X.; Shen, Y.; Wu, H. Antibacterial Mechanisms of Silica/Polydopamine/Silver Nanoparticles against Gram Positive and Gram Negative Bacteria. *Micro Nano Lett.* **2014**, *9* (3), 210–214.

(42) Mhatre, E.; Troszok, A.; Gallegos-Monterrosa, R.; Lindstädt, S.; Hölscher, T.; Kuipers, O. P.; Kovács, Á. T. The Impact of Manganese on Biofilm Development of Bacillus Subtilis. *Microbiology* **2016**, *162* (8), 1468–1478.

(43) Stöckel, S.; Meisel, S.; Böhme, R.; Elschner, M.; Rösch, P.; Popp, J. Effect of Supplementary Manganese on the Sporulation of textitBacillus Endospores Analysed by Raman Spectroscopy: Raman Study of the Effect of Manganese on the Sporulation of textitBacillus Endospores. *J. Raman Spectrosc.* **2009**, *40* (11), 1469–1477.

(44) Stephenson, K.; Lewis, R. Molecular Insights into the Initiation of Sporulation in Gram-Positive Bacteria: New Technologies for an Old Phenomenon. *FEMS Microbiol. Rev.* **2005**, *29* (2), 281–301.

(45) Nicholson, W. L. Roles of Bacillus Endospores in the Environment. *Cell. Mol. Life Sci.* **2002**, *59* (3), 410–416.

(46) Yang, Y.; Wu, H.-J.; Lin, L.; Zhu, Q.; Borriss, R.; Gao, X.-W. A Plasmid-Born Rap-Phr System Regulates Surfactin Production, Sporulation and Genetic Competence in the Heterologous Host, Bacillus Subtilis OKB105. *Appl. Microbiol. Biotechnol.* **2015**, *99* (17), 7241–7252.

(47) McKenney, P. T.; Driks, A.; Eichenberger, P. The Bacillus Subtilis Endospore: Assembly and Functions of the Multilayered Coat. *Nat. Rev. Microbiol.* **2012**, *11* (1), 33–44.

(48) CHARNEY, J.; FISHER, W. P.; HEGARTY, C. P. Managanese as an Essential Element for Sporulation in the Genus Bacillus. *J. Bacteriol.* **1951**, *62* (2), 145–148.

(49) Vasantha, N.; Freese, E. The Role of Manganese in Growth and Sporulation of Bacillus Subtilis. *J. Gen. Microbiol.* **1979**, *112* (2), 329–336.

(50) Hachisuka, Y.; Imura, H.; Nakata, A.; Hattori, E. Sporulation Promoting Factor in Vegetative Cells of textitBacillus Subtilis. *Microbiol. Immunol.* **1983**, *27* (12), 1005–1019.

(51) Vater, J.; Kablitz, B.; Wilde, C.; Franke, P.; Mehta, N.; Cameotra, S. S. Matrix-Assisted Laser Desorption Ionization--Time of Flight Mass Spectrometry of Lipopeptide Biosurfactants in Whole Cells and Culture Filtrates of Bacillus Subtilis C-1 Isolated from Petroleum Sludge. *Appl. Environ. Microbiol.* **2002**, *68* (12), 6210–6219.

(52) Cooper, D. G.; Macdonald, C. R.; Duff, S. J.; Kosaric, N. Enhanced Production of Surfactin from Bacillus Subtilis by Continuous Product Removal and Metal Cation Additions. *Appl. Environ. Microbiol.* **1981**, *42* (3), 408–412.

(53) Cawoy, H.; Mariutto, M.; Henry, G.; Fisher, C.; Vasilyeva, N.; Thonart, P.; Dommes, J.; Ongena, M. Plant Defense Stimulation by Natural Isolates of *Bacillus* Depends on Efficient Surfactin Production. *Mol. Plant-Microbe Interact.* **2014**, *27* (2), 87–100.

(54) Mulligan, C. N.; Yong, R. N.; Gibbs, B. F. Heavy Metal Removal from Sediments by Biosurfactants. *J. Hazard. Mater.* **2001**, *85* (1–2), 111–125.

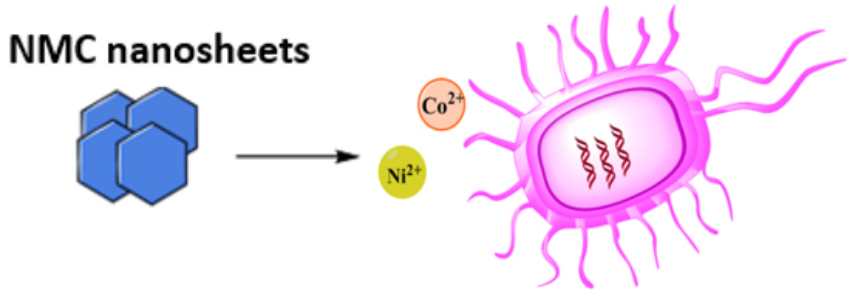

109x42mm (150 x 150 DPI)